Wind Energ. Sci. Discuss., https://doi.org/10.5194/wes-2018-27
Manuscript under review for journal Wind Energ. Sci.
Discussion started: 26 April 2018

WIND ENERGY SCIENCE DISCUSSIONS

Optimal Output Feedback H_∞ Torque Control of a Wind Turbine Rotor using a Parametrically Scheduled Model

Dana Martin[1], Kathryn Johnson[1], Christopher Bay[1,2], Daniel Zalkind[2], Lucy Pao[2], Meghan Kaminski[3], and Eric Loth[3]

[1]Colorado School of Mines Golden, CO 80401
[2]University of Colorado Boulder, CO 80309
[3]University of Virginia, VA 22904

Correspondence to: Dana Martin (dmartin@mymail.mines.edu)

Abstract. Wind turbines are nonlinear, time-varying systems that are subject and sensitive to model parameter variations and a stochastic wind field. For such applications, Linear Parameter Varying (LPV) control provides a state-space approach to designing nonlinear controllers with robust performance. LPV uses multi-input multi-output (MIMO) model with a guaranteed limit on the exogenous disturbance's gain with respect to performance signals. A robust matrix inequality synthesis of an H_∞ based performance LPV controller using a parametrically varying model will be developed with the goal of obtaining a torque controller with drive-train damping properties. The technique guarantees a-priori performance values and closed-loop stability for the simplified model, and provides a systematic tuning procedure to adjust controller performance.

1 Introduction

Wind turbine technology has emerged as the most competitive form of renewable energy production (REN21, 2017, 2016) during the green push over the past two decades, and the evolution of wind energy control systems continue to enable the advancement of turbine technology. Wind energy increased its penetration into the electricity grid around the world with a record 63 GW of wind generation added during 2015 and 55 GW during 2016, equating to a 22% and 12% respective growth on the world market compared to previous years' statistics (REN21, 2017, 2016). Wind offers a renewable alternative to carbon-based energy sources with the promise of lowering carbon emissions by 2,700 tons of CO_2 per year per 1.5 MW turbine, which is the equivalent of planting 4 square kilometers of forest each year (REN21, 2016). While renewable growth had record numbers during 2015 with 2016 coming in a close second, the Energy Information Administration (EIA) predicts that the U.S. wind power capacity would have to reach more than 300 GW to achieve the 20% wind-generated electricity by 2030, which would result in a displacement of 50% electric utility natural gas consumption and 18% coal consumption (of Energy Efficiency and Energy, 2008). To meet 20% by 2030, the U.S. needs to increase its wind power penetration by 265% of its current capacity, equivalent to an additional 218 GW of wind power (REN21, 2016, 2017)(of Energy Efficiency and Energy, 2008). With so much growth still to come in the next decade, the market is ripe for emerging technologies to further improve the viability and impact of wind energy on the world market by further decreasing the levelized cost of energy

Wind Energ. Sci. Discuss., https://doi.org/10.5194/wes-2018-27
Manuscript under review for journal Wind Energ. Sci.
Discussion started: 26 April 2018

(LCOE). One such technology with the ability to improve existing wind turbine operation, in addition to enabling advanced turbine technology is the control system.

Nonlinear dynamics and modeling uncertainties of wind turbines make non-linear and gain scheduling methodology necessary for optimal operation across all wind speeds. However, non-linear control architectures do not easily lend themselves to multi-input multi-output (MIMO) controller synthesis, and lack the theory for a-priori guarantees of stability (Shamma, 1988). To address the immediate industry needs of improving performance prediction and decreasing the number of under-performing, short-lived turbines (Fields et al., 2016), Linear Parameter Varying (LPV) control can be utilized for both increasing performance and the longevity of turbine life (Adegas and Stoustrup, 2012; Inthamoussou et al., 2016; Sloth et al., 2011).

When formulated using a state-space representation, it is conducive to MIMO control synthesis satisfying multiple control objectives and robust performance. This formulation allows the designer to ensure stability given plant parameter uncertainty, and uncertainties in the measured scheduling parameter (Shamma, 1988; Zhao and Nagamune, 2017; Sato and Peaucelle, 2013; Sato et al., 2010). LPV control theory can utilize H_2 and H_∞ (Levine, 2011) concepts during the construction of the optimization problem, giving it the ideal combination of the robustness of H control and optimal performance across a wide operating envelope. However, the range of the operating envelope also contributes to the nonlinearity of the optimization model, and with below-rated operation of a variable speed wind turbine, solving the optimization is not always trivial due to the dimensionality of the problem. For this reason, methods such as the gridding technique and slack variable approach can be used to create feasible solutions to once infeasible optimization problems allowing existing conic solver algorithms (Sturm, 1999) to find globally feasible solutions (Ostergaard et al., 2009).

Most recent work regarding LPV control of wind turbines has focused on variable pitch systems due to their prevalence in the industry and increased controllability. A detailed derivation of LPV control schemes for Region 2 (below rated) and Region 3 (above rated) wind conditions is given in (Bianchi et al., 2006). The authors develop a LPV model that is scheduled on the wind speed, generator speed, and blade pitch angle. This leads to the development of conventional single-input single-output (SISO) controllers for turbine speed control in Region 3 and generator torque control in Region 2. Bianchi, et al. then develop a MIMO controller that gives increased power performance (smoothed generator output) without increased pitch actuation while substantially reducing torque fluctuations. Finally, the authors present a method for combining the two MIMO LPV controllers to provide control over the entire operating envelope.

Others have also proposed LPV controllers for operation across the wind envelope for turbines. A switching LPV controller for a variable speed and pitch turbine was presented in (Lescher et al., 2006). The main objective of this controller was to reduce drivetrain torsion, blade and tower flexion. This control scheme is then compared against conventional PI controllers and a gain scheduled LQG controller, showing reduced mechanical fatigue in the system while maintaining power output.

Further extending the objectives in operating wind turbines, work has been done with LPV-based active power control (APC). In (Inthamoussou et al., 2016), the authors develop an LPV controller within the standard decoupled pitch and torque control structure. The controller is scheduled on pitch and power demand, thus not depending on wind speed measurements. The controller was simulated in FAST on the NREL 5MW benchmark turbine (Jonkman et al., 2009), compared against gain scheduled PI and H_∞ controllers, the LPV controller outperformed the others in terms of APC while providing a decrease in

Wind Energ. Sci. Discuss., https://doi.org/10.5194/wes-2018-27
Manuscript under review for journal Wind Energ. Sci.
Discussion started: 26 April 2018

aerodynamic loads. While the above works showcase several of the benefits of LPV control for wind turbines, the simulations were done with a traditional three-bladed, upwind turbine. The two-bladed, downwind configurations are unexplored with regard to LPV control.

The contributions of this paper lie in a drive train damper utilizing only output feedback of the generator speed angular velocity as opposed to state-feedback (Darrow et al., 2011), comparisons of controller derivation and performance to existing methods (Ostergaard et al., 2009), detailed modeling, and implementation of a robust linear matrix inequality (LMI) approach to gain scheduled, output feedback torque control of a Segmented Ultra-light Morphing Rotor (Loth et al., 2017). The control synthesis methodology to be developed in the following paper lends itself to a generalized plant that can be modeled using aerodynamic basis functions (Mohammadpour and Scherer, 2012) and simplified linear models to arrive at a working torque controller for a full degree of freedom (DOF), non-linear plant.

In this paper the authors will propose, synthesize, and implement an LMI based LPV controller using H_∞ performance specifications for below-rated operation with the aim of increasing power capture at low wind speeds and reducing component loads. The paper will be organized as follows. Section 2 will derive a simplified, two mass model of the rotor and drive train, which will be used in Section 3 to synthesize an optimal LPV controller using an H_∞ performance metric. Section 4 will provide below rated, turbulent inflow simulation results and data analysis to quantify controller performance. Finally, Section 5 gives closing remarks.

2 Modeling

2.1 Three state drive-train model

In order to implement a model-based controller to damp drive-train oscillations, a simplified turbine model needs to be derived. Using a flexible drive-train model of the low-speed shaft (LSS), gear box with ratio N_g, and high speed shaft (HSS) as depicted in Figure 1, torque balances on either side of the gear box are performed to develop the relationship between generated aerodynamic torque Q_a, drive-train torsion and applied generator torque τ_g.

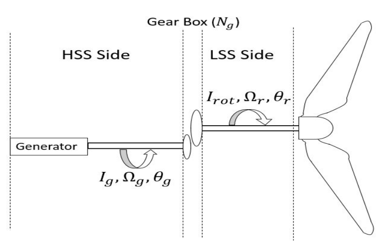

Figure 1. The flexible, two mass drive-train model. The section labeled HSS depicts the high speed shaft side of the gear box with a rotational inertia I_g, angular velocity Ω_g, an azimuthal position of θ_g. The gear box ratio (N_g) section is the gearing connecting the HSS and LSS masses of the drive-train. The section labeled LSS depicts the low speed shaft side of the drive-train connected directly to the rotor with a rotational inertia I_r, angular velocity Ω_r and azimuthal position of θ_r. The model assumes a drive-train with no frictional damping.

Wind Energ. Sci. Discuss., https://doi.org/10.5194/wes-2018-27
Manuscript under review for journal Wind Energ. Sci.
Discussion started: 26 April 2018

Figure 1 depicts a two mass model of the rotor, with the gear box connecting the LSS mass (denoted using subscript rot) and the HSS mass (denoted using subscript g). Equation (1) describes the torque balance on the LSS side of the gear box with Q_a being the aerodynamic torque generated by the wind on the rotor, and (2) describes the torque balance on the HSS side of the gear box where Q_{LSS} represents the torque applied by the LSS through the gear box.

$$I_{rot}\dot{\Omega}_r(t) = Q_a(t) - Q_{LSS} \tag{1}$$

$$I_g\dot{\Omega}_g = Q_{HSS} - \tau_g \tag{2}$$

The LSS torque can also be computed using the drive-train torsional spring constant, k_d, torsional damping constant, C_d, and a difference in azimuthal position (ϕ) and angular velocities (Ω) of the two masses across the gear box as shown in (3).

$$Q_{LSS} = \frac{k_d}{N_g}(\phi_r - \phi_g) + C_d(\frac{\Omega_r}{N_g} - \frac{\Omega_g}{N_g^2}) \tag{3}$$

The generated aerodynamic torque given an operating point ($|_{OP}$) can be linearly approximated as a function of rotor speed (Ω_r), blade pitch (β), and free stream wind speed (V_∞) as

$$Q_a(\Omega_r,\beta,V_\infty) = \bar{Q}_a|_{OP} + \left.\frac{\partial Q_a}{\partial \Omega_r}\right|_{OP}\delta\Omega_r + \left.\frac{\partial Q_a}{\partial \beta}\right|_{OP}\delta\beta + \left.\frac{\partial Q_a}{\partial V_\infty}\right|_{OP}\delta V_\infty. \tag{4}$$

Equation (4) includes the nominal aerodynamic torque, $\bar{Q}_a|_{OP}$, for a given operating point plus the sensitivities around that operating point, which vary according to the selected local operating point. The operator δ indicates deviation of a variable from its local operating point.

The final form of the 3 DOF system's dynamics formulated into state-space format are given by (5).

$$\begin{bmatrix}\dot{x}_1\\ \dot{x}_2\\ \dot{x}_3\end{bmatrix} = \begin{bmatrix}\frac{\frac{\partial Q_a}{\partial \Omega_r}|_{OP} - C_d}{I_{rot}} & \frac{-k_d}{I_{rot}} & \frac{C_d}{I_{rot}N_g}\\ 1 & 0 & \frac{-1}{N_g}\\ \frac{C_d}{I_gN_g} & \frac{k_d}{I_gN_g} & \frac{-C_d}{I_gN_g^2}\end{bmatrix}\begin{bmatrix}x_1\\ x_2\\ x_3\end{bmatrix} + \begin{bmatrix}0 & \left.\frac{\partial Q_a}{\partial \beta}\right|_{OP}\frac{1}{I_{rot}}\\ 0 & 0\\ \frac{-1}{I_g} & 0\end{bmatrix}\begin{bmatrix}\delta\tau_g\\ \delta\beta\end{bmatrix} + \begin{bmatrix}\left.\frac{\partial Q_a}{\partial V_\infty}\right|_{OP}\frac{1}{I_{rot}}\\ 0\\ 0\end{bmatrix}\delta V_\infty \tag{5}$$

where the state vector is given by (6).

$$\begin{bmatrix}x_1\\ x_2\\ x_3\end{bmatrix} = \begin{bmatrix}\delta\Omega_r\\ (\phi_r - \phi_g)\\ \delta\Omega_g\end{bmatrix} \tag{6}$$

The partial derivatives of aerodynamic torque are not constant throughout the entire operating range of a wind turbine. Thus, the system dynamics defined in (5) vary according to wind speed, which will be developed in Section 2.2.

2.2 Basis Functions

Torque control of a wind turbine is not stationary because the dynamics of the turbine differ according to the inflow velocity. The controller must be able to follow an operating trajectory as opposed to maintaining a single operating point. Since the partial derivatives of aerodynamic torque (4), with respect to the three independent variables (Ω_r, β, V_∞) vary throughout the operating envelope, they can provide the parametric variation required for LPV controller synthesis. Figure 2 shows these variations as functions of free stream wind speed at selected turbine operating points along the partial load operating trajectory in below-rated conditions.

Table 1. Operating points of the turbine used to calculate the operating points and A, B, B_w dependence on wind speed corresponding to the below-rated trajectory of the turbine.

V_∞ (m/s)	Ω_r (rpm)	τ_g (N-m)	β (deg)
2	7.273	58	0.5
3	11.72	140	0.5
4	15.77	274.2	0.5
5	21.97	410	0.5

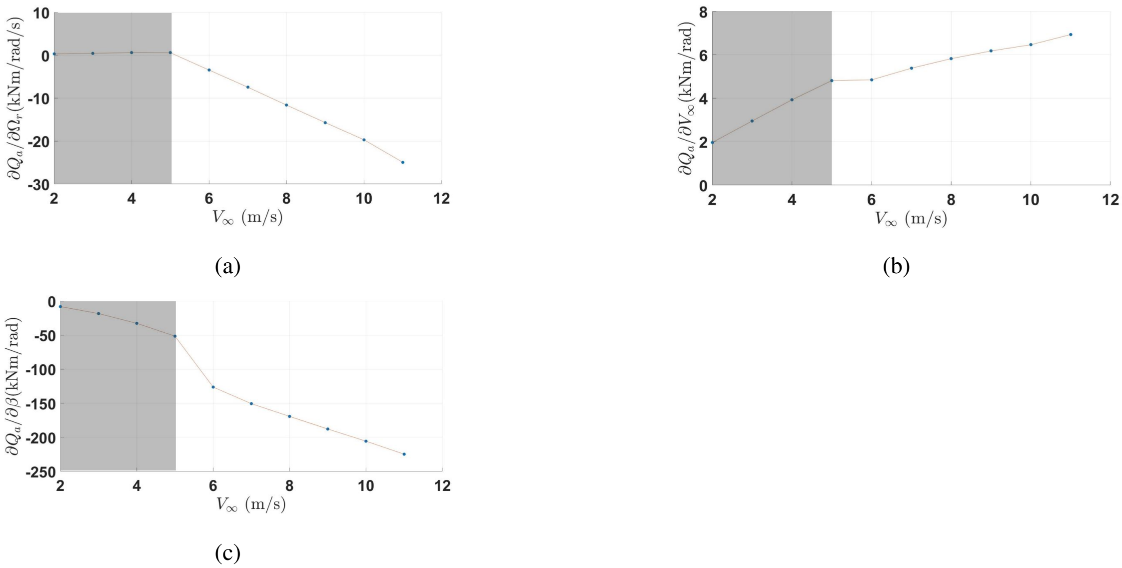

Figure 2. Partial derivative for aerodynamic torque approximation (4). Subplot (a) shows variation of $\frac{\partial Q_a}{\partial \Omega_r}$ with V_∞. Subplot (b) shows variation of $\frac{\partial Q_a}{\partial V_\infty}$ with V_∞. Subplot (c) shows variation of $\frac{\partial Q_a}{\partial \beta}$ with V_∞. The portion of the sensitivities corresponding to below-rated operating points is indicated by the shaded gray box.

This paper is focused on partial load operation (region II) (Johnson et al., 2006), therefore, only the portion of the sensitivities falling between the cut-in (2 m/s) and rated (5 m/s) wind speeds will be used in the construction of the parameter varying functions. The turbine under study is a scaled design that has resulted in very low wind speed operation. See Section 4.1 for more information. Due to the required assumptions of affine dependence for system scheduling (Ostergaard et al., 2009), only

Wind Energ. Sci. Discuss., https://doi.org/10.5194/wes-2018-27
Manuscript under review for journal Wind Energ. Sci.
Discussion started: 26 April 2018

first order interpolation functions will be used for scheduling of system dynamics. That is,

$$\rho_1(\theta_{1-4}) = \frac{\partial Q_a}{\partial \Omega_r}(\theta_{1-4}) \approx \xi_{\rho_1}\theta_{1-4} + \kappa_{\rho_1} \tag{7}$$

$$\rho_2(\theta_{1-4}) = \frac{\partial Q_a}{\partial V_\infty}(\theta_{1-4}) \approx \xi_{\rho_2}\theta_{1-4} + \kappa_{\rho_2} \tag{8}$$

$$\rho_3(\theta_{1-4}) = \frac{\partial Q_a}{\partial \beta}(\theta_{1-4}) \approx \xi_{\rho_3}\theta_{1-4} + \kappa_{\rho_3}. \tag{9}$$

where (θ_i) denotes the slope of the aerodynamic sensitivity scheduled on the linearizations performed at operating points corresponding to $i = 2, 3, 4,$ and 5 m/s wind speeds along the operating trajectory corresponding to the optimal tip speed ratio (λ_*) tracking (Johnson et al., 2006).

3 Controller Derivation

Controller performance and closed-loop performance depends on the selection of the channels and weights used in the optimization. This specific structure of system definition creates the versatility exhibited by performance channel based control, creating the ability to develop a systematic frequency domain design method for plant performance during time domain operation. Since this paper is concerned with below-rated operation of the wind turbine, the performance of the plant is achieved through applied generator torque. The torque signal aims to counteract the generated aerodynamic torque acting within the plane of the rotor, maintaining the rotor's optimum tip-speed ratio during turbulent inflow. The turbulent inflow contains a wide spectrum of frequencies, and performance channel design gives the control designer the ability to shape closed-loop response depending on the excitation frequency. For torque control, the controller must be able to track optimal tip speed ratio given a low frequency excitation, but also be able to constrain component loading for natural harmonics of the plant components. For this specific application, drive-train loads are of special interest, as they are a major cause of turbine downtime (Shang, 2013).

3.1 System Definition

To synthesize the control gain a parameter dependent, continuous-time, state-space system is defined as shown in (10), where the quantitative matrix entries were derived and shown in (5).

$$\begin{aligned}
\dot{x}(t) &= A(\theta(t))x(t) + B_u(\theta(t))u(t) + B_w(\theta(t))w(t) \\
z(t) &= C_z(\theta(t))x(t) + D_{zu}(\theta(t))u(t) + D_{zw}(\theta(t))w(t) \\
y(t) &= C_y(\theta(t))x(t) + D_{yw}(\theta(t))w(t)
\end{aligned} \tag{10}$$

Where $x \in \mathbb{R}^{m\times 1}$, $u \in \mathbb{R}^{n\times 1}$, $w \in \mathbb{R}^{q\times 1}$ are the system states, control inputs and exogenous disturbances, respectively. For the sake of space and notational simplicity, the scheduling parameter's time dependence will be dropped for the remainder of the paper. The system matrices have corresponding dimensions. C_z is a weighting matrix from states to the performance vector z, which is used during the optimization process. The matrices defined in the performance vector equation heavily influence the feasibility of the optimization problem and the overall controller performance. In essence, the definition of the performance vector defines the minimization. In defining this vector, LPV theory (Shamma, 1988; Sato and Peaucelle, 2013; Mohammadpour and Scherer, 2012) allows the designer to place an upper limit on the gain from the exogenous disturbance, $w(t)$, to the selected performance channels. This H_∞ performance metric is:

$$\sup_{\theta\in\Omega_\theta, w\in\mathscr{L}_2, w\neq 0} \frac{||z(t)||_2}{||w(t)||_2} < \gamma_\infty. \tag{11}$$

To apply the theory in (Shamma, 1988; Sato and Peaucelle, 2013; Mohammadpour and Scherer, 2012), the scheduling parameter θ, its rate of variation $\dot{\theta}$, uncertainty in the scheduling parameter δ_θ, and its rate of variation $\dot{\delta}_\theta$ must all lie within known, bounded sets with upper and lower bounds defined by the control designer.

$$\begin{aligned}
\theta \in \Omega_\theta, \Omega_\theta &:= \left\{\underline{\theta} < \theta < \bar{\theta}\right\}\\
\dot{\theta} \in \Lambda_\theta, \Lambda_\theta &:= \left\{\underline{\dot{\theta}} < \dot{\theta} < \bar{\dot{\theta}}\right\}\\
\delta_\theta \in \Omega_{\delta_\theta}, \Omega_{\delta_\theta} &:= \left\{\underline{\delta_\theta} < \delta_\theta < \bar{\delta_\theta}\right\}\\
\dot{\delta}_\theta \in \Lambda_{\delta_\theta}, \Lambda_{\delta_\theta} &:= \left\{\underline{\dot{\delta}_\theta} < \dot{\delta}_\theta < \bar{\dot{\delta}}_\theta\right\}
\end{aligned} \tag{12}$$

The upper $\bar{(\cdot)}$ and lower $\underline{(\cdot)}$ bounds on the scheduling parameter (θ) are fixed during the aerodynamic design of the physical plant, being the cut-in wind speed up to the rated wind speed, while the upper and lower bounds on the scheduling parameter's rate of variation must encompass the highest and lowest frequency component of the turbulent inflow. For this application the hub height free stream wind speed is assumed to be perfectly measurable using a meteorological tower mounted anemometer, resulting in a measured bias error of 0 for the uncertainty (δ_θ) in the measured scheduling parameter. The authors recognize that this assumption could prohibit the application of this control architecture on a physical turbine. However, areas of research such as LIDAR (Scholbrock et al., 2016) are increasing the accuracy of wind speed prediction and robust forms of LPV theory (Zhao and Nagamune, 2017) can be utilized in future work to address the shortcoming introduced by this assumption. In the following section, the LMI system will be developed and used for the synthesis of the control matrices.

3.2 Performance Vector Design

The design of the performance vector z is essential to controller performance. For below-rated, variable speed turbine operation, the controller's main objective is λ_* tracking using the applied generator torque τ_g. The regulation of generator speed is a single input, single output (SISO) system, however; to achieve load reduction, generator speed regulation will be accompanied by an additional objective of reducing drive-train torsional oscillations as compared to a baseline control architecture.

Similar to H_∞ control design, the closed-loop system response can be shaped using weighting and sensitivity functions to influence system response in the frequency domain. The goal of a torsional drive-train damper is to reduce the torsional oscillations induced by differences in LSS and HSS azimuthal positions and angular velocities as modeled in (10), which can be achieved through the use of a bandpass filter centered at the drive-train first eigen-frequency ($\Xi_{DT_{1P}}$). $\Xi_{DT_{1P}}$ can be determined using a FAST linearization (Jonkman and Buhl, 2005) with the flexible drive-train DOF enabled. By examining

Wind Energ. Sci. Discuss., https://doi.org/10.5194/wes-2018-27
Manuscript under review for journal Wind Energ. Sci.
Discussion started: 26 April 2018

the eigenvalue of the linearized A matrix corresponding to the flexible drive-train state, the eigen-frequency can be identified using (13) and via frequency response Figure (3).

$$\Xi_{DT_{1P}} = \sqrt{\zeta_{real}^2 + \zeta_{imag}^2} \tag{13}$$

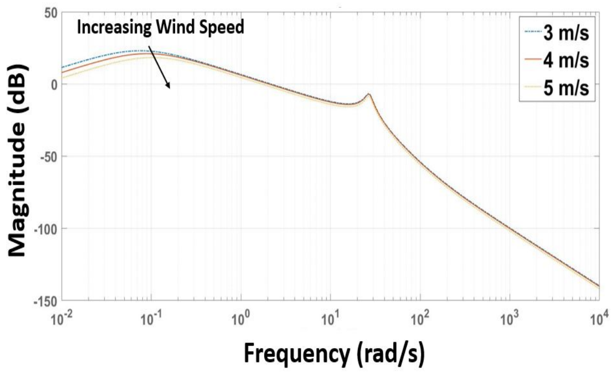

Figure 3. Magnitude frequency response of the transfer function from inflow to drive-train angular velocity torsion.

With the eigen-frequency of the drive-train known, the bandpass filter denoted by W_{z1}, can be designed following methods outlined in (Sugiura et al., 2013) and (Mohammadpour and Scherer, 2012) which will be used to shape the closed-loop system response. This closed-loop shaping is accomplished by multiplying the transfer function of the bandpass filter W_{z1} with the sensitivity function ($S = (I + G_p)^{-1}$) where G_p is the transfer function from the horizontal inflow wind to rotor angular velocity without any closed-loop control, and the transfer function from the inflow wind (V_∞) to rotor speed (Ω_r) is G_v (Mohammadpour and Scherer, 2012). In addition to penalizing 1P drive-train torsions, high frequency variations in the torque control signal will be penalized using a first order high-pass filter (W_u) with a cutoff frequency set above the 2P frequency to reduce control actuation for excitation frequencies above the 1p harmonic. A plot of the frequency response for the performance vector is shown below in Figure 4.

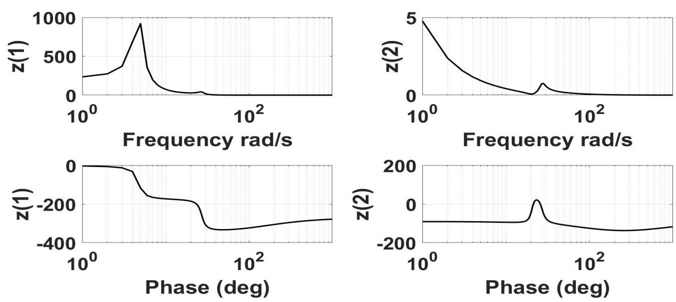

Figure 4. Frequency response for weighting functions used for closed-loop shaping. Plots show $z(1)$ denoting the drive-train torsion band-pass filter for a given inflow excitation frequency and $z(2)$ represents a low-pass filter penalizing high frequency generator torque control action for a given inflow field.

Wind Energ. Sci. Discuss., https://doi.org/10.5194/wes-2018-27
Manuscript under review for journal Wind Energ. Sci.
Discussion started: 26 April 2018

The design of z is done using transfer functions residing in the frequency domain, resulting in high order models that can't be applied to the original 3 state system. The increase in model order results from the loop-shaping process , introducing pole-zero pairs that can be removed due to cancellations. This pole-zero pair removal can be accomplished utilizing model reduction techniques (Laub et al., 1987; Laub, 1980; Gawronski and Juang, 1990; Moore, 1981) to arrive at a system having the same order as (10) with desired closed-loop characteristics as is depicted in Figure 5.

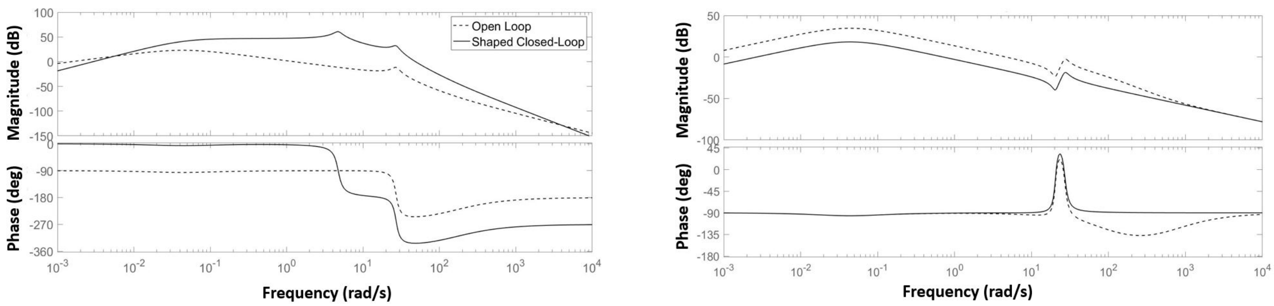

(a) (b)

Figure 5. Comparison of open-loop and shaped closed-loop frequency response. Figure (a) shows plots for transfer function from inflow wind to drive train torsion. Figure (b) shows frequency response for transfer function from inflow wind to rotor angular velocity.

The loop shaping process results in transfer function with high order polynomials, and in turn, pole zero pairs. Since the optimization process will be performed in the time domain, the transfer functions depicted in Figures 5(a) and 5(b) will be converted to time domain matrices C_z and D_{zu} to be used in the definition of $z(t)$ given in (10). The introduction of the pole-zero pairs during the shaping process (14), and the conversion from the frequency to the time domain, results in a system with incompatible dimensions, as $x \in \mathbb{R}^{m\times 1} \implies C \in \mathbb{R}^{p\times m}$. For this reason, reduction techniques as previously mentioned, aim to eliminate states produced during the frequency domain multiplication having small gramian values, in turn, having little influence on the system. During the model reduction procedure, the DC gain of the full order model must match the DC gain of the reduced order model, as this influences the controller performance and step response.

With the matrices C_z, D_{zu}, and D_{zw} defining the performance vector z given by (10) designed, the optimization problem becomes a weighted, closed-loop sensitivity minimization for the two signal system shown in (14).

$$\left\| \begin{matrix} W_{z1}SG_p \\ W_uSG_v \end{matrix} \right\|_\infty . \tag{14}$$

3.3 H_∞ Performance Constraint

Briefly mentioned earlier, LPV control theory (Shamma, 1988; Mohammadpour and Scherer, 2012; Levine, 2011) allows designers to guarantee closed-loop stability and define an a-priori upper bound on defined performance metrics (14) by designing a controller scheduled for dynamic operation across the non-linear operating envelope of the plant. LPV is a form of quasi-nonlinear control theory utilizing linear time-invariant (LTI) state-space formulation of the plant dynamics and H robust

Wind Energ. Sci. Discuss., https://doi.org/10.5194/wes-2018-27
Manuscript under review for journal Wind Energ. Sci.
Discussion started: 26 April 2018

control theory for optimal plant operation. For an optimal, output-feedback controller the following control law is defined:

$$\begin{aligned} \dot{x}_c(t) &= A_c(\theta)x_c(t) + B_c(\theta)y(t) \\ u(t) &= C_c x_c(t) + D_c y(t). \end{aligned} \tag{15}$$

The scheduling of the controller is contained within $A_c(\theta)$ and $B_c(\theta)$ as denoted by their dependence on the scheduling parameter θ, and it is assumed that C_c and D_c are constant, ensuring convexity during the optimization process. The LPV controller given by (15) can be represented in matrix form as

$$\bar{K}(\theta)\left\{ \begin{bmatrix} \dot{x}_c(t) \\ u(t) \end{bmatrix} = \begin{bmatrix} A_c(\theta) & B_c(\theta) \\ C_c & D_c \end{bmatrix} \begin{bmatrix} x_c(t) \\ y(t) \end{bmatrix} \right. . \tag{16}$$

Substituting the definition of $u(t)$ given by (15) into (10), the closed-loop system's dynamics are computed as (Mohammadpour and Scherer, 2012)

$$\begin{aligned} A_{cl}(\theta, \theta+\delta_\theta) &= \bar{A}(\theta) + \bar{B}_u \bar{K}(\theta, \theta+\delta_\theta)\bar{C}_y \\ B_{cl}(\theta, \theta+\delta_\theta) &= \bar{B}_w + \bar{B}_u \bar{K}(\theta, \theta+\delta_\theta)\bar{D}_{yw}(\theta) \\ C_{cl}(\theta, \theta+\delta_\theta) &= \bar{C}_z(\theta) + \bar{D}_{zu}(\theta)\bar{K}(\theta+\delta_\theta)\bar{C}_y \\ D_{cl}(\theta, \theta+\delta_\theta) &= \bar{D}_{zw}(\theta) + \bar{D}_{zu}(\theta)\bar{K}(\theta+\delta_\theta)\bar{D}_{yw}(\theta) \end{aligned} \tag{17}$$

where the closed-loop state vector $x_{cl} = \begin{bmatrix} x \\ x_c \end{bmatrix}$ and the following matrix definitions ensure appropriate dimensions

$$\left[\begin{array}{c|c|c} \bar{A}(\theta) & \bar{B}_w(\theta) & \bar{B}_u \\ \hline \bar{C}_z(\theta) & \bar{D}_{zw}(\theta) & \bar{D}_{zu}(\theta) \\ \hline \bar{C}_y & \bar{D}_{yw}(\theta) & \end{array}\right] = \left[\begin{array}{cc|c|cc} A(\theta) & \mathbf{0} & B_w(\theta) & \mathbf{0} & B_u \\ \mathbf{0} & \mathbf{0} & \mathbf{0} & I_n & \mathbf{0} \\ \hline C_z(\theta) & \mathbf{0} & D_{zw}(\theta) & \mathbf{0} & D_{zu}(\theta) \\ \hline \mathbf{0} & I_n & \mathbf{0} & & \\ C_y & \mathbf{0} & D_{yw}(\theta) & & \end{array}\right] \tag{18}$$

The final closed-loop system is given by (19).

$$\begin{aligned} \dot{x}_{cl} &= A_{cl}x_{cl} + B_{cl}u \\ y &= C_{cl}x_{cl} + D_{cl}u \end{aligned} \tag{19}$$

Using the performance bound (11), the optimization measure (14), the closed-loop system matrices (17) and (18), and a Lyapunov stability approach (Levine, 2011), the practical constraints can be constructed and implemented using the closed set containing the operating envelope of the plant (12). For closed-loop stability and performance, it is necessary that the LMI (20) be satisfied during the optimization problem.

Wind Energ. Sci. Discuss., https://doi.org/10.5194/wes-2018-27
Manuscript under review for journal Wind Energ. Sci.
Discussion started: 26 April 2018

$$\begin{bmatrix} A_{cl}(\theta)^T X_{cl} + X_{cl} A_{cl}(\theta) & X_{cl} B_w(\theta) & C_{cl}(\theta)^T \\ B_{cl}(\theta)^T X_{cl} & -\gamma_\infty^2 I & D_{zw}(\theta)^T \\ C_{cl}(\theta) & D_{zw}(\theta) & -I \end{bmatrix} \prec 0 \tag{20}$$

The upper left entry of (20) utilizes a Lyapunov matrix X, with the closed-loop matrix A_{cl}, to ensure loop stability. In traditional nonlinear control, the matrix X_{cl} is unknown and the solution gives the nonlinear controller providing closed-loop stability. In the derivation of an LPV controller, this same approach is utilized in parallel with (11) to derive the nonlinear controller (16) ensuring stability and performance.

3.4 Practical Implementation

In the previous sections, the underlying theory for nonlinear stability and performance was developed. In the following section, the practical implementation considerations for robust gain scheduled output feedback (GSOF) controller synthesis will be presented. The practical implementation of the system differs from the given constraint of (20), in the aspect that (20) is actually a bilinear matrix inequality (BMI) and is very difficult to solve, even for today's advanced conic solvers. Secondly, it is often the case that condition numbers of wind turbine state space matrices pose ill-conditioned matrices, causing numerical instabilities leading to infeasible optimization problems, or controllers which cannot be re-constructed from the obtained optimization variables (Ostergaard et al., 2009). This procedure and implementation facilitates the synthesis and tuning of a drive-train damping torque controller for an arbitrary wind turbine with a model as given by (5).

For an H_∞ control type problem the entries of the LMI (Υ_d, Γ_D), $(\Upsilon_u(\theta+\delta_\theta), \Gamma_u)$, $\Upsilon_A(\theta, \theta+\delta)$, $\Upsilon_B(\theta, \theta+\delta)$, $\Upsilon_C(\theta, \theta+\delta)$, $\Upsilon_D(\theta, \theta+\delta)$, and $\Upsilon_X(\theta, \dot{\theta}, \delta, \dot{\delta})$ are defined in (Mohammadpour and Scherer, 2012). The above notation, closed-loop system definitions, and (20) provide the final form of the LMI (21) to be used for the synthesis of the controller (15). The variables ϵ_1, $\mathscr{E}$, and $\mathscr{L}$ arise from the factorization of the Lyapunov matrix (Sato and Peaucelle, 2013; Sato et al., 2010), and presence of uncertainty in the scheduling parameter (Petersen, 1987).

$$\Upsilon_\infty(\theta, \dot{\theta}, \delta_\theta, \dot{\delta}_\theta) = \begin{bmatrix} \Upsilon_A(\theta, \theta+\delta_\theta) + \Upsilon_A(\theta, \theta+\delta_\theta)^T + \Upsilon_X(\theta, \dot{\theta}, \delta_\theta, \dot{\delta}_\theta) & \Upsilon_C(\theta, \theta+\delta_\theta)^T & \Upsilon_B(\theta, \theta+\delta_\theta) \\ \star & -\gamma_\infty I_{n_z} & \Upsilon_D(\theta, \theta+\delta_\theta) \\ \star & \star & -\gamma_\infty I_{n_w} \end{bmatrix} \tag{21}$$

Where $\star$ denotes a symmetric matrix block. Using (21), the final form of the inequality constraint for robust optimization is given by (22) and (23), providing a robust implementation of optimization constraints stemming from the constraint (20)

Wind Energ. Sci. Discuss., https://doi.org/10.5194/wes-2018-27
Manuscript under review for journal Wind Energ. Sci.
Discussion started: 26 April 2018

(Mohammadpour and Scherer, 2012).

$$\begin{bmatrix} \mathscr{H} & I_n \\ I_n & \mathscr{L} \end{bmatrix} > 0 \tag{22}$$

$$\begin{bmatrix} \Upsilon_\infty(\theta,\dot{\theta},\delta_\theta,\dot{\delta}_\theta) & \star \\ \begin{bmatrix} \Upsilon_d(\theta,\dot{\theta},\delta_\theta,\dot{\delta}_\theta) & \mathbf{0} & \mathbf{0} \\ \Upsilon_u(\theta,\dot{\theta},\delta_\theta,\dot{\delta}_\theta) & \mathbf{0} & \mathbf{0} \end{bmatrix} & \begin{bmatrix} \Gamma_d(\theta,\delta_\theta) & \mathbf{0} \\ \mathbf{0} & \Gamma_u \end{bmatrix} \end{bmatrix} < 0 \tag{23}$$

3.5 Optimization

The optimization measure and constraints developed in Sections 3.4 and 3.3 provide a framework for generalized turbine torque controller synthesis and robust optimization implementation. The region of feasible solutions is constrained by the a-priori definition and ranges of the scheduling parameter θ in conjunction with the ranges in uncertainty of the scheduling parameter δ_θ (12). While the procedure outlined in Section 3.4 is robust, it is still a bilinear matrix inequality (BMI) despite the congruence transformation described in (Levine, 2011) due to the multiplication of matrix variables ϵ_1, $\mathscr{E}_2$ and $\mathscr{L}$. The evolution of conic solvers (Sturm, 1999) have catalyzed the use of LPV controllers, however, solving a BMI is still much more computationally expensive than solving an LMI. For that reason, practical assumptions using arbitrarily chosen values for the aforementioned matrix variables can be assigned to reduce BMI's to LMI's.

4 Simulation

LPV design has many advantages to traditional gain scheduling due to its a-priori guarantees of stability and performance for nonlinear systems. However, these guarantees and performance criterion can only be applied to the LPV model used in the controller synthesis process (5). While ensuring stability of the closed-loop model used for controller synthesis validates theory, the performance of the controller when applied to the actual wind turbine plant may differ because of its additional non-linearities, plant parameter differences, and exogenous disturbance assumption (12). Therefore, the controller performance will be tested within the aeroelastic simulation tool FAST (Jonkman and Buhl, 2005).

4.1 Turbine Description

Controller performance evaluation was conducted as applied to the Segmented Ultra-light Morphed Rotor - Demonstrator (SUMR-D). This rotor is a Gravo-Aeroelasticly Scaled (GAS) model (Loth et al., 2018; Kaminski et al., 2018) of the 100-meter blade SUMR-13i (Ananda et al., 2018; Martin et al., 2017; Martin and Zalkind, 2016; Zalkind et al., 2017) down-wind, two-bladed rotor with a pre-aligned rotor (Loth et al., 2017). This scaling method aims to fully capture the key dynamics of the full-scale model with an emphasis on matching the non-dimensional flapping frequency, moment ratios, flapping tip deflection and design tip speed ratio. The blades are first geometrically scaled by a length scaling factor (η) defined as

$$\eta = \frac{R_s}{R_f} \tag{24}$$

Wind Energ. Sci. Discuss., https://doi.org/10.5194/wes-2018-27
Manuscript under review for journal Wind Energ. Sci.
Discussion started: 26 April 2018

where the subscript s refers to the scaled model, the subscript f refers to the full-scale model, and R represents the blade length.

With SUMR-D having a blade length of 20.87 m, $\eta = 0.2$, which is then applied to all external dimensions of the blade. The rotational speed is scaled by keeping the ratio of centrifugal to gravitational moments constant ($\frac{M_c}{M_G} = \frac{R\Omega^2 cos(\Psi)}{g}$). This speed scaling allows the blade dynamics to remain similar through the full rotation of the turbine blade, resulting in the scaled angular velocity of the rotor given by (25).

$$\Omega_s = \frac{\Omega_f}{\sqrt{\eta}} \tag{25}$$

Table 2. SUMR-13i and SUMR-D Turbine Parameters.

	SUMR-13i	SUMR-D
Length Scaling Factor (η)	1	0.2
Design Blade Mass (kg)	54,787	625
Cut-in Wind Speed (m/s)	5	2
Rated Wind Speed (m/s)	11.3	5
Cut-out Wind Speed (m/s)	25	11
λ^*	9.5	9.5
Rated Rotor Speed (rpm)	9.82	21.96
Rated Power (MW)	13.2	0.0389

4.2 Baseline Case and Simulated Environment

The baseline case will be a torque look-up table control scheme (BL) as described in (Martin et al., 2017; Zalkind et al., 2017) and applied to the same SUMR-D rotor. The inflow conditions to be simulated fall within Design Load Cases 1.1 and 1.2 as defined in IEC 61400-1 (IEC, 2005). Turbulence characteristics as generated by TurbSim (Jonkman and Kilcher, 2006) are representative of turbulence characteristics as experienced at the National Wind Technology Center (NWTC) in Boulder, CO. The site requires class I-A turbulence analysis, and 600 second turbulent wind files with a mean wind speed of 4 m/s, which is within the SUMR-D's below-rated operating range. Furthermore, all data channel names and axis conventions follow those used by FAST (Jonkman and Buhl, 2005).

4.3 Turbulent Inflow

A sample time series plot of the controller performance is shown in Figures 6. Examining the plot, periods of drive-train damping are observed as compared with the baseline controller especially around t=125s, but there is not a clear overall difference for the entire time series. A statistical analysis of the variance for the load channels depicted in Figure (6) paints a clearer picture with LSS torsional moment (LSSMxa) of the DT controller having a 10.71% lower variance than the BL,

Wind Energ. Sci. Discuss., https://doi.org/10.5194/wes-2018-27
Manuscript under review for journal Wind Energ. Sci.
Discussion started: 26 April 2018

Table 3. Data channel variance (σ) comparison. The values in the table compare the percent difference between the two controllers (BL and LPV) computed using $frac(LPV - BL)BL$.

$\Delta\sigma_{LSSMxa}$	$\Delta\sigma_{TwrBaseMxt}$	$\Delta\sigma_{TwrBaseMyt}$	$\Delta\sigma_{GenPower}$
-10.71%	-30.54%	19.95%	17.01%

the tower base side-to-side (TwrBsMxt) moment having a 30.54% lower variance, while the tower base fore-aft (TwrBsMyt) moment has a 19.95% larger variance than the BL controller. The reduction in the in-plane loads is due to the LPV controller applied generator torque aiming to maintain the rotor's angular velocity and minimize torsional oscillations between the LSS and HSS, all acting within the plane of the rotor.

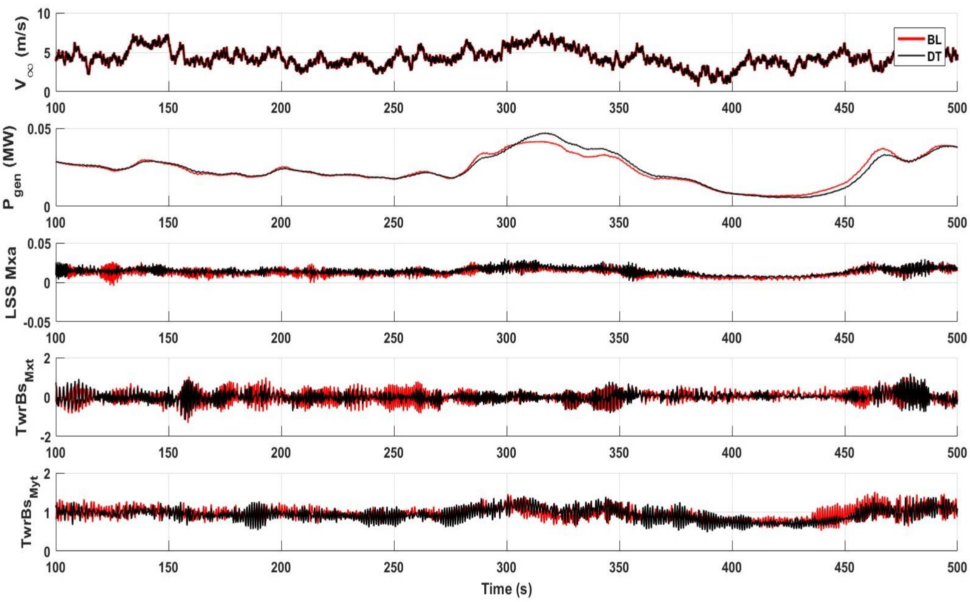

Figure 6. Time-series comparison of Generator Power P_{gen}, LSS torsional $LSSMxa$ moment, tower base side-to-side $TwrBs_{Mxt}$ bending moment given in (MN-m), and tower base fore-aft $TwrBs_{Myt}$ bending moment given in (MN-m) for a turbulent inflow with a mean wind speed of 4 m/s.

As stated in Section 3.2, the torque controller's main goal during below-rated operation is to track the design λ^*. Figure 7 depicts a time series plot showing real time λ^* tracking computed using (26) where *i* denotes the instantaneous parameter value.

$$\lambda^i = \frac{\Omega_r^i * R}{V_\infty^i} \tag{26}$$

The mean value of λ as tracked for the BL controller is 10.44 while the DT controller maintains a mean value of 9.09, with the variances being 9.22 and 7.20 respectively. From this, it can be concluded that the DT controller tracks the turbine closer to λ^* than the BL, resulting in a more efficient energy production. At approximately 375 seconds, the tip speed ratio (λ) plot shows a huge spike in λ, corresponding to a dip in wind speed which can be seen in Figure 6, however, the magnitude of the event is limited through LPV control action.

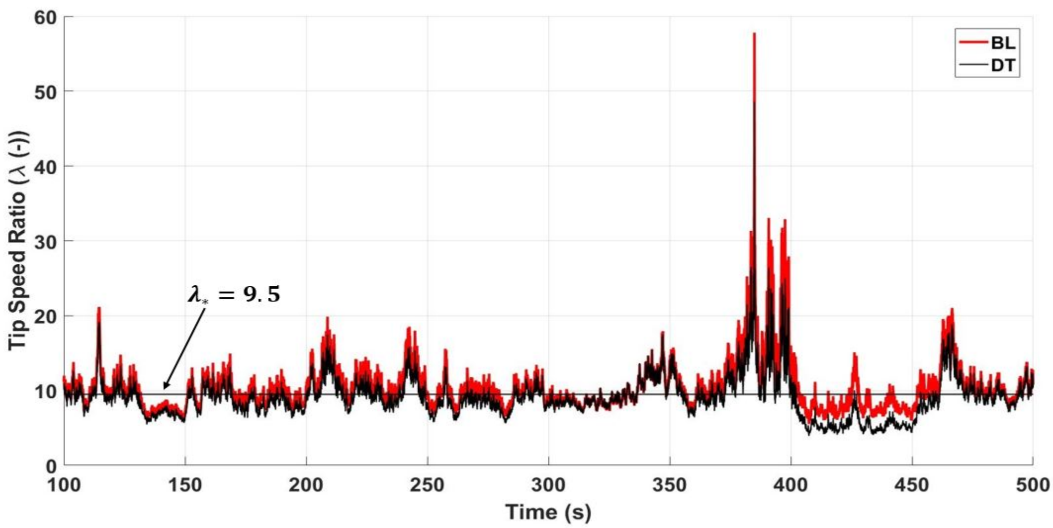

Figure 7. Time-series plot showing the tip speed ratio as tracked during a turbulent inflow with a mean inflow of 4 m/s.

Analysis presented in this section provided insight to the DT controller's ability to limit oscillations in LSS torsion, and its ability to track λ^* resulting in efficient energy production. To further quantify the DT controllers performance in terms of fatigue load reduction, Damage Equivalent Loads (DEL) will be used as a metric for multiple load channels to view fatigue distribution as viewed from the entire turbine's perspective with additional wind input files used for the analysis to increase the statistical significance of the results.

4.4 DEL Analysis

As all systems, wind turbines are subject to the conservation of energy, and with decreases in targeted load channels, there may be increases in other load channels. The fatigue analysis on turbine components is performed using six turbulent inflow files generated using unique seeds, each with a mean wind velocity of 4 m/s. Results are processed using the rain-flow algorithm available through MLife (Hayman and Jr., 2012). The maximum allowable load used during the rain-flow counting was computed according to a maximum allowable strain calculation for carbon and glass materials used in the material lay up specified by the structural designer and presented in (Griffith and Ashwill, 2011) applied to the SUMR-D blade. Figure 8 shows a comparison of aggregate damage equivalent load (DEL) between the BL and DT controllers.

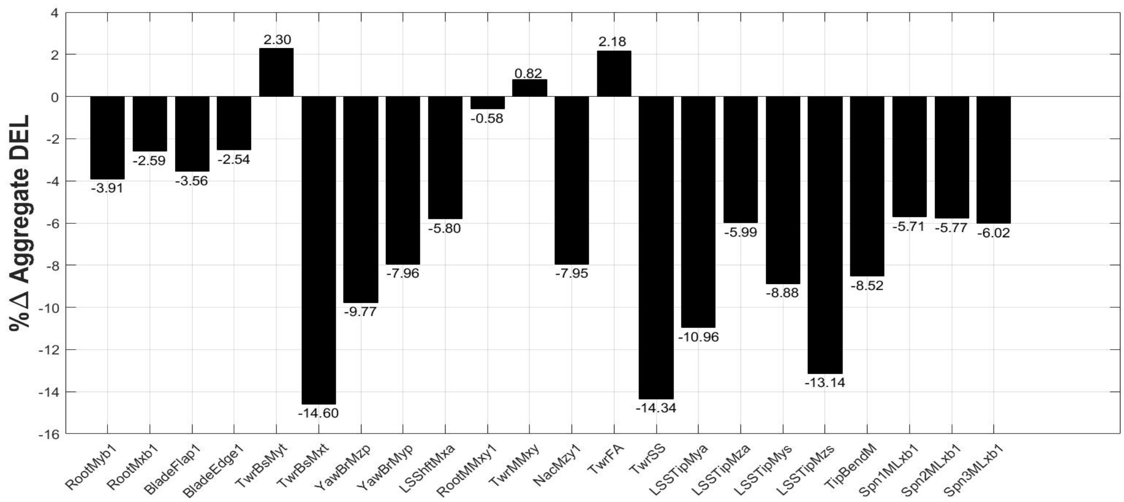

Figure 8. Comparison of Aggregate DEL with fixed means.

A negative $\%\Delta$ represents a reduction in the specified load channel for the DT controller as compared to the average of the six runs of the BL controller with the same inflow files. Trends in Figure 8 reaffirm the variance analysis of the time-series data with decreases in DEL for almost all of the in-plane loads. The LPV DT controller was able to reduce the LSS torsional DEL by 6.20%, the tower base side-to-side DEL by 14.77%, but with an unfortunate increase in tower base fore-aft DEL of 8.38%. The increase in tower base fore-aft bending moment DEL is not surprising, as the main driver behind out-of-plane loads are driven by thrust force, requiring pitch actuation for substantial influence.

5 Conclusions and Future Work

In this paper the authors derived a simplified, parametrically scheduled wind turbine model used in the synthesis of an LPV controller. The controller was synthesized utilizing an H_∞ performance metric for the shaped closed-loop response as defined by the performance vector during Region II power production. A robust optimization architecture inspired by (Mohammadpour and Scherer, 2012) was used for the synthesis of an optimal, dynamic control law (15) and controller performance was quantified as applied to the SUMR-D turbine rotor during turbulent inflow conditions representative of turbulence as seen at the NWTC testing site. Time-series data for a turbulent inflow with a mean wind speed of 4 m/s was used to quantify advanced control performance as compared to the baseline case. Data analysis showed decreases in DEL torsional LSS moments along with tower base side-to-side moments resulting from increased control actuation during 1P oscillations due to differences in HSS and LSS angular velocity and position. The output feedback architecture presented in this paper relies on a simplified model describing dynamic coupling between the LSS and HSS, and a loop shaping performance vector to provide targeted load channel damping using the readily available HSS angular velocity signal, providing fatigue reduction results.

Future work to be completed includes the field testing of the LPV controller as applied to the National Wind Technology Center's CART2 turbine with the SUMR-D rotor, application of the controller on the extreme scale SUMR-13i rotor Ananda et al. (2018), application of the controller on additional extreme-scale segmented ultra-light morphing rotors, and the design and optimization of an above-rated pitch controller, which will focus on the reduction of out-of-plane loads.

Wind Energ. Sci. Discuss., https://doi.org/10.5194/wes-2018-27
Manuscript under review for journal Wind Energ. Sci.
Discussion started: 26 April 2018

5 Bibliography

Adegas, F. D. and Stoustrup, J.: Structured Control of LPV Systems with Application to Wind Turbines, American Control Conference, 2012.

Ananda, G. K., Bansal, S., and Selig, M. S.: Aerodynamic Design of the 13.2 MW SUMR-13i Wind Turbine Rotor, AIAA SciTech Forum, 2018.

Bianchi, F. D., Battista, H. d., and Mantz, R. J.: Wind Turbine Control Systems: Principles, Modelling and Gain Scheduling Design, Springer, London, 2007 edition edn., 2006.

Darrow, J., Johnson, K., and Wright, A.: Design of a tower and drive train damping controller for the three-bladed controls advanced research turbine operating in design-driving load cases, Wind Energy, 14, 571–601, 2011.

Fields, J., Tinnesand, H., and Baring-Gould, I.: Distributed Wind Resource: State of the Industry, Tech. Rep. 5000-66419, National Renewable Energy Laboratory Technical Report, Golden, CO, 2016.

Gawronski, W. and Juang, J. N.: Model Reduction in Limited Time and Frequency Intervals, International Journal of Systems Science, 21, 349–376, 1990.

Griffith, D. T. and Ashwill, T. D.: The Sandia 100-meter All-glass Baseline Wind Turbine Blade: SNL100-00, SAND2011-3779, 2011.

Hayman, G. J. and Jr., M. B.: MLife User's Manual Version 1.00, National Renewable Energy Laboratory, Golden, CO, 2012.

IEC: IEC 61400-1 International Standard, International Electrotechnical Commission, 3 edn., 2005.

Inthamoussou, F. A., Battista, H. D., and Mantz, R. J.: LPV-based active power control of wind turbines covering the complete wind speed range, Renewable Energy, 99, 996–1007, 2016.

Johnson, K. E., Pao, L. Y., Balas, M. J., and Fingresh, L. J.: Control of Variable Speed Wind Turbines: Standard and Adaptive Techniques for Maximizing Energy Capture, *IEEE Control System Magazine*, 26, 2006.

Jonkman, B. J. and Kilcher, L.: TurbSim User's Guide: Version 1.06.00, National Renewable Energy Laboratory, Golden, CO, nrel/tp-500-39797 edn., 2006.

Jonkman, J. and Buhl, M. L.: FAST User's Guide, National Renewable Energy Laboratory, Golden, CO, 2005.

Jonkman, J., Butterfield, S., Musial, W., and Scott, G.: Definition of a 5MW Reference Wind Turbine for Offshore System Development, Technical Report TP-500-38060, National Renewable Energy Laboratory (NREL), 2009.

Kaminski, M., Loth, E., Qin, C., and Griffith, D. T.: Gravo-Aeroelastic Scaling a 13.2 MW Wind Turbine Blade to a 1-Meter Model, AIAA SciTech Forum, 2018.

Laub, A. J.: Computation of Balancing Transformations, Proceedings of the American Control Conference, 1980.

Laub, A. J., Heath, M. T., Paige, C. C., and Ward, R. C.: Computation of System Balancing Transformations -and Other Applications of Simultaneous Diagonalization Algorithms, IEEE Transactions on Automatic Control, pp. 115–122, 1987.

Lescher, F., Zhao, J. Y., and Borne, P.: Switching LPV Controllers for a Variable Speed Pitch Regulated Wind Turbine, in: The Proceedings of the Multiconference on "Computational Engineering in Systems Applications", vol. 2, pp. 1334–1340, https://doi.org/10.1109/CESA.2006.4281844, 2006.

Levine, W. S.: Control System Advanced Methods, Taylor and Francis Group, 2011.

Loth, E., Steele, A., Ichter, C. Q. B., Selig, M. S., and Moriarty, P.: Downwind pre-aligned rotors for extreme-scale wind turbines, Wind Energy, 20, 1241–1259, 2017.

Loth, E., Kaminski, M., Qin, C., Fingresh, L. J., and Griffith, D. T.: Gravo-Aeroelastic Scaling for Extreme-Scale Wind Turbines, AIAA SciTech Forum, 2018.

Martin, D. and Zalkind, D.: 50 MW Segmented Ultralight Morphing Rotor (SUMR): Design Concept and Controls Strategies, https://www.slideshare.net/sandiaecis/dana-martindaniel-zalkind-50-mw-segmented-ultralight-morphing-rotor-sumr-design-concept-and-controls-strategies', 2016.

Martin, D. P., Johnson, K. E., Zalkind, D. S., and Pao, L. Y.: LPV-Based Torque Control for an Extreme-Scale Morphing Wind Turbine Rotor, *American Control Conference*, 2017.

Mohammadpour, J. and Scherer, C.: Control of Linear Parameter Varying Systems with Applications, Springer, Boston, MA, 2012.

Moore, B.: Principal Component Analysis in Linear Systems: Controllability, Observability, and Model Reduction, IEEE Transactions on Automatic Control, pp. 17–31, 1981.

of Energy Efficiency, U. D. O. and Energy, R.: Wind Energy by 2030: Increasing Wind Energy's Contribution to U.S. Electric Supply, https://www.nrel.gov/docs/fy08osti/41869.pdf, 2008.

Ostergaard, K. Z., Stroustrup, J., and Brath, P.: Linear paramter varying control of wind turbines covering both partial laod and full load conditions, *International Journal of Robust and Nonlinear Control*, 2009.

Petersen, I. R.: A stabilization algorithm for a class of uncertain linear systems, Systems & Control Letters, 8, 351–357, 1987.

REN21: Renewables 2016 Global Status Report, http://www.ren21.net/wp-content/uploads/2016/06/GSR_2016_Full_Report.pdf', 2016.

REN21: Renewables 2017 Global Status Report, http://www.ren21.net/wp-content/uploads/2017/06/17-8399_GSR_2017_Full_Report_0621_Opt.pdf', 2017.

Sato, M. and Peaucelle, D.: Gain-scheduled output-feedback controllers using inexact scheduling parameters for continuous-time LPV systems, Automatica, 49, 2013.

Sato, M., Ebihara, Y., and Peaucelle, D.: Gain Scheduled state-feedback controllers using inexactly measured scheduling parameters: H_2 and H_∞ problems, In: Proceedings of the American control conference, pp. 3094–3099, 2010.

Scholbrock, A., Flemming, P., Wright, A., Wang, N., Schlipf, D., and Johnson, K.: Lidar-Enhanced Wind Turbine Control: Past, Present, and Future, NREL/CP-5000-65879, 2016.

Shamma, J.: Analysis and design of gain scheduled control systems, Ph.D. thesis, Massachusetts Institute of Technology, 77 Massachusetts Ave, 1988.

Shang, S.: Report on Wind Turbine Subsystem Reliability: A Survey of Various Databases, National Renewable Energy Laboratory, Golden, CO, nrel/pr-5000-59111 edn., 2013.

Sloth, C., Esbensen, T., and Stoustrup, J.: Robust and fault-tolerant linear parameter-varying control of wind turbines, *Mechatronics*, 21, 645–659, 2011.

Sturm, J. F.: Using SeDuMi 1.02, A Matlab toolbox for optimization over symmetric cones, Optimization Methods and Software, 11, 625–653, https://doi.org/10.1080/10556789908805766, https://doi.org/10.1080/10556789908805766, 1999.

Sugiura, Y., Kawamura, A., and Iiguni, Y.: Performance Analysis of an Inverse Notch Filter and Its Application to F_0 Estimation, Circuits and System, 2013.

Zalkind, D. S., Pao, L. Y., Martin, D. P., and Johnson, K. E.: Models used for the simulation and control of a segmented ultralight morphing rotor, The International Federation of Automatic Control, 2017.

Zhao, P. and Nagamune, R.: Switching LPV controller design under uncertain scheduling parameters, Automatica, 76, 243–250, 2017.